Received August 31, 2019, accepted September 12, 2019, date of publication September 17, 2019,
date of current version September 26, 2019.

Digital Object Identifier 10.1109/ACCESS.2019.2941909

Probability Assessment of Characteristics of Sub-Synchronous Oscillation in D-PMSG-Based Wind Power Generation System

SHUN TAO[1], (Member, IEEE), LEI ZHAO[1], (Member, IEEE), KUNYU LIAO[2], AND YUNBO LIU[1]
[1]State Key Laboratory for Alternate Electrical Power System with Renewable Energy Sources, North China Electric Power University, Beijing 102206, China
[2]Suzhou Power Supply Company, State Grid Jiangsu Electric Power Company Ltd., Suzhou 215004, China

Corresponding author: Lei Zhao (ZhaoLeicyjx@163.com)

ABSTRACT In recent years, sub-synchronous oscillation (SSO) phenomena occur in direct-drive permanent magnet synchronous generator (D-PMSG) based wind power generation systems (WPGS) in many regions of China. The SSO characteristics, frequency and damping, are all time-varying mostly affected by changes of wind speed and D-PMSGs number. It is the importance for the design of SSO suppression to know the variation ranges of characteristics and the risk of unstable SSO. The small signal model of the D-PMSG-based WPGS is firstly established in this paper, considering the functional relationship between wind speed and wind turbine output power. Based on the small signal model and the probability distribution function (PDF) of wind speed, the SSO probability assessment method with the least square method (LSM) polynomial fitting is then proposed. Therefore, the probability distributions of SSO frequency and damping considering wind speed variation are obtained efficiently. By PSCAD/EMTDC simulations and comparisons, the obtained results with the eigenvalue analysis method based on the small signal model are certificated. Then the probability assessment method is applied to study the influences of different average wind speeds under different number of D-PMSGs on the probability distribution of SSO frequency and damping. The changes of SSO frequency bandwidth and the risk of unstable SSO are depicted relative completely. The variation range of SSO frequency is consistent with the actual accident scenario in Hami area of Xinjiang, China.

INDEX TERMS Direct-drive permanent magnet synchronous generator (D-PMSG), probability assessment, sub-synchronous oscillation (SSO), wind speed.

I. INTRODUCTION

In recent years, with the consumption of traditional fossil energy such as coal, oil, and natural gas, environmental problems have become increasingly serious, and the large-scale development and utilization of renewable energy have become the consensus of the world [1]. New energy power generation technologies represented by wind power have been widely used worldwide. However, the oscillation stability problems associated with wind turbines (WTs) have occurred in many regions of China.

In July 2015, the severe sub-synchronous oscillation (SSO) with no series compensation condition occurred in the wind farm based on D-PMSGs in Hami area of Xinjiang, China [2].

The associate editor coordinating the review of this manuscript and approving it for publication was Jason Gu.

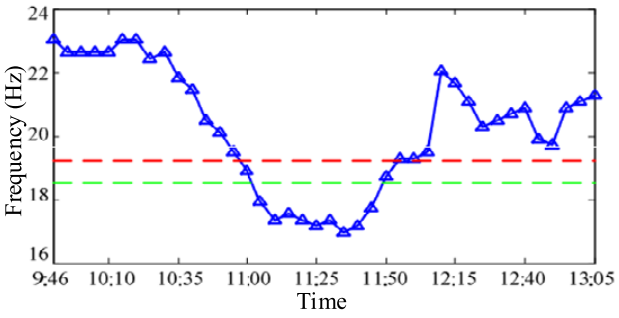

FIGURE 1. SSO frequency in Hami area of Xinjiang, China.

The change of the SSO frequency in the line during a certain period of the day is shown in Fig. 1 [3]. It can be seen that the SSO frequency of the current changes continuously in real time, and the variation range is from 17Hz to 23 Hz,

indicating that the SSO has time-varying characteristics. The parameters of controller, the number of WTs, the output power of each WT, and the reactance of the grid connection have influences on the characteristics of SSO [2]–[5]. But the two main factors which cause the characteristics of SSO to change with time are the output power of each WT and the number of WTs [6]. The output power of each WT is closely related to the wind speed [2], [7], and the randomness of the wind speed has the most significant affection on the time-varying characteristics of SSO [8].

Therefore, it is necessary to use an uncertain analysis method to simulate the stochastic characteristics of wind speed and quantitatively assess the SSO frequency and damping probability distribution characteristics of D-PMSG. Currently, the uncertainty studies of wind power focus on power prediction [15], [16], probabilistic power flow calculation [17], [18] and small interference stability [19], [20]. However, the uncertainty research has just been involved in the study of wind power system SSO. Reference [8] used the probabilistic collocation method to assess the safety risk of SSO of wind power farms; In [21], [22], a probabilistic method is applied to study the influencing factors and the suppression measures of sub-synchronous control interaction. However, the research objects in these literatures are all DFIG-based WPGS. In [23], the probability distributions of SSO frequency and damping are estimated with the Gaussian mixture model of D-PMSG-based WPGS, but the influences of the number of WTs and the wind speed on the SSO frequency and damping probability distributions are not analyzed individually.

In order to study the time-varying characteristics of SSO, it is necessary to first quantify the influence of determined wind speed on SSO. There are frequency sweeping method [9], impedance analysis method [4], [12], time domain simulation method [10] and eigenvalue analysis method [11]. As the SSO frequency bandwidth of D-PMSG-based WPGS caused by wind speed is relatively narrow [2], the oscillation frequencies may not be found by the frequency sweep method setting an unsuitable frequency increment. Because the impedance analysis method ignores the characteristics of controller parameter asymmetry and AC-DC side dynamic coupling, it is difficult to accurately model and analyze the influence of wind speed on SSO [13]. As for the eigenvalue analysis method, which is a rigorous and accurate analysis method based on linear system theory [14], it can be used to accurately analyze the characteristics of SSO under a determined wind speed operation condition.

This paper oriented D-PMSG-based WPGS establishes a small signal model by utilizing the functional relationship between wind speed and output power of WT. Based on the model and the least square method (LSM) polynomial fitting, the relationship of SSO frequency and wind speed as well as the relationship of damping and wind speed within wind speed range for WT operation are obtained. Then the probability assessment method of SSO characteristics is established by introducing the probability distribution of wind speed. The small signal model quantitatively analyzes the influences of wind speed change on SSO frequency and damping, and its accuracy is validated with the comparisons of PSCAD/EMTDC simulations. Based on the probability assessment method, the effects of the different average wind speeds under different number of WTs on the probability distributions of SSO frequency and damping are studied. The SSO frequency fluctuation range consistent with the actual accident scenario in Hami is reproduced as well. Those conclusions can contribute on suppression design and risk estimation of unstable SSO.

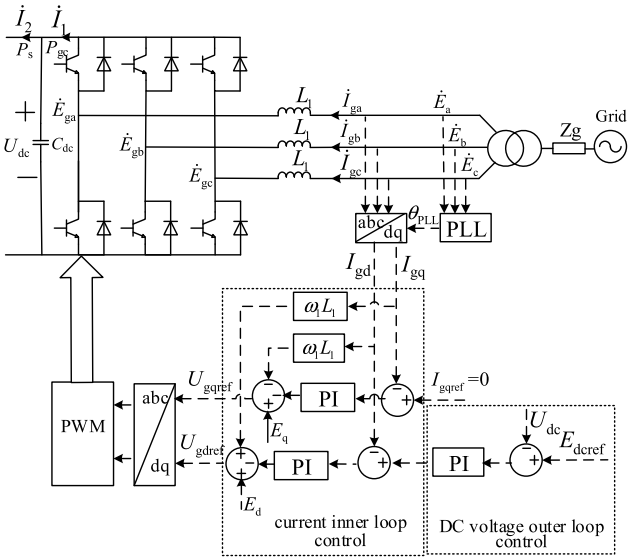

FIGURE 2. Equivalent circuit and control diagram of D-PMSG-based WPGS.

II. D-PMSG EQUIVALENT MODEL

A D-PMSG mainly consists of a WT, a permanent magnet synchronous generator (PMSG), a machine-side converter (MSC), a grid-side converter (GSC), a DC link and a L filter [4], [24]. Between the MSC and GSC, there is a DC link to separate the convertors without affecting each other, and the on-grid dynamics of a D-PMSG mainly depends on the control features of its GSC [2]. Therefore, the D-PMSG is generally equivalent to a voltage source converter (VSC) [13], [25]–[27], as shown in Fig. 2.

Fig. 2 consists of two parts: the equivalent circuit and the control loops. The GSC of D-PMSG is connected to the infinite grid through a filter link L_1, a transformer, and a grid connection reactance Z_g. The current reference direction is from the grid to the PMSG [13]. The control loop is oriented at the grid voltage in the dq frame system, including the DC voltage outer loop, the current inner loop, and the phase-locked loop (PLL). The controllers of current inner loop and the DC voltage outer loop adopt proportional integral (PI) control.

In Fig. 2, $\dot{E}_{ga}$, $\dot{E}_{gb}$, and $\dot{E}_{gc}$ are the voltages of GSC outlet; $\dot{I}_{ga}$, $\dot{I}_{gb}$, and $\dot{I}_{gc}$ are the GSC output currents; $\dot{E}_a$, $\dot{E}_b$, and $\dot{E}_c$ are the voltages of the grid-connected point, which are all in the three-phase stationary coordinate system and respectively

converted to U_{gd} and U_{gq}, I_{gd} and I_{gq}, E_d and E_q in the dq frame by Park transformation.

III. METHODOLOGY

The methodology is presented by two parts: the small signal model of D-PMSG-based WPGS and the SSO probability assessment method, and the former is the basis of the latter.

A. SMALL SIGNAL MODEL

The small signal model of a D-PMSG-based WPGS is established in the form of per-unit value. Besides the consideration of the DC voltage control loop, the current inner loop, the phase-locked loop and the filter link, the model takes a wind speed variable into account by using the functional relationship between wind speed and output power of WT, to accurately quantify the influences of wind speed on the SSO frequency and damping of the system.

The actual power P_{tur} obtained by WT is closely related to the wind speed v. When the wind speed is higher than the rated value and lower than the cut-out value, P_{tur} is the rated power P_{rate} by changing the pitch; when the wind speed is lower than the rated value and higher than the cut-in value, the pitch angle $\beta = 0°$, the WT achieves maximum power point tracking (MPPT) to keep the wind energy utilization coefficient C_p at the maximum value and constant (generally 0.593). The functional relationship between P_{tur} and v is [24]:

$$P_{tur} = \begin{cases} 0, & v \in [0, v_{cut\text{-}in}) \\ 0.5\pi R_{tur}^2 \rho C_p v^3 = k_1 v^3, & v \in [v_{cut\text{-}in}, v_{rated}] \\ P_{rate}, & v \in (v_{rated}, v_{cut\text{-}out}] \end{cases} \quad (1)$$

where, R_{tur} is the radius of the WT blade, ρ is the air density, v_{cut-in} is the cut-in wind speed and $v_{cut-out}$ is the cut-out wind speed. The blade radius of the WT is a constant and the air density is normally assumed as a constant in the same area, thus k_1 in (1) is a constant coefficient.

Considering the power loss of the PMSG and MSC, the conversion efficiency is assumed as a constant value k_2. Thus, the active power transmitted from the MSC to the DC bus is:

$$P_s = k_2 P_{tur}/P_0 \quad (2)$$

where P_0 is the capacity base value of the system.

The active power transmitted by GSC is:

$$P_{gc} = I_{gd} U_{gd} + I_{gq} U_{gq} \quad (3)$$

Ignoring the DC side resistance, it is assumed that the active power is transmitted from the DC bus to the GSC without any loss.

The dynamic equation of the DC capacitor is [13]:

$$s(U_{dc} - U_{dc0}) = \frac{(P_{gc} - P_s)\,\omega_b}{U_{dc} C_{dc}} \quad (4)$$

where, U_{dc} is the monitoring DC voltage value, U_{dc0} is the DC voltage in per-unit at steady state, ω_b is the angular frequency reference value, and C_{dc} is the DC side capacitance in per-unit.

Therefore the state equation of U_{dc} is,

$$\frac{dU_{dc}}{dt} = \frac{(P_{gc} - P_s)\,\omega_b}{U_{dc} C_{dc}} \quad (5)$$

The control and the circuit state equations of each part of the D-PMSG-based WPGS can be written as the general form of (6) [28], [29]:

$$\begin{cases} \dfrac{d\boldsymbol{x}}{dt} = \mathbf{f}(\boldsymbol{x}, \boldsymbol{y}) \\ \mathbf{0} = \mathbf{g}(\boldsymbol{x}, \boldsymbol{y}) \end{cases} \quad (6)$$

where, $\boldsymbol{x}$ is a state variable vector and $\boldsymbol{y}$ is an algebraic variable vector; $\mathbf{f}(\cdot)$ and $\mathbf{g}(\cdot)$ are differential equations and algebraic equations, respectively.

Based on Lyapunov's first theorem, the small disturbance stability of system is analyzed, and (6) is linearized at a certain operating balance point $(\boldsymbol{x_0}, \boldsymbol{y_0})$, which can be expressed as

$$\begin{cases} \frac{d}{dt}\Delta\boldsymbol{x} = \tilde{\mathbf{A}}\Delta\boldsymbol{x} + \tilde{\mathbf{B}}\Delta\boldsymbol{y} \\ \mathbf{0} = \tilde{\mathbf{C}}\Delta\boldsymbol{x} + \tilde{\mathbf{D}}\Delta\boldsymbol{y} \end{cases} \quad (7)$$

where, $\begin{cases} \tilde{\mathbf{A}} = \left(\dfrac{\partial \mathbf{f}(\boldsymbol{x},\boldsymbol{y})}{\partial \boldsymbol{x}}\right)_{\boldsymbol{x}_0,\boldsymbol{y}_0} & \tilde{\mathbf{B}} = \left(\dfrac{\partial \mathbf{f}(\boldsymbol{x},\boldsymbol{y})}{\partial \boldsymbol{y}}\right)_{\boldsymbol{x}_0,\boldsymbol{y}_0} \\ \tilde{\mathbf{C}} = \left(\dfrac{\partial \mathbf{g}(\boldsymbol{x},\boldsymbol{y})}{\partial \boldsymbol{x}}\right)_{\boldsymbol{x}_0,\boldsymbol{y}_0} & \tilde{\mathbf{D}} = \left(\dfrac{\partial \mathbf{g}(\boldsymbol{x},\boldsymbol{y})}{\partial \boldsymbol{y}}\right)_{\boldsymbol{x}_0,\boldsymbol{y}_0} \end{cases}$

By eliminating $\Delta\boldsymbol{y}$ from (7),

$$\frac{d}{dt}\Delta\boldsymbol{x} = \mathbf{A}\Delta\boldsymbol{x} \quad (8)$$

where, $\mathbf{A} = \tilde{\mathbf{A}} - \tilde{\mathbf{B}}\tilde{\mathbf{D}}^{-1}\tilde{\mathbf{C}}$ is the coefficient matrix of (7), and the stability of the system can be analyzed by calculating the eigenvalues of the matrix $\mathbf{A}$.

B. SSO PROBABILITY ASSESSMENT METHOD

Based on the eigenvalue analysis results of the small signal model, the least square method is used for polynomial fitting, which can efficiently and accurately obtain the fitting functional relationship between wind speed and SSO frequency or damping. Introduce the probability density function (PDF) of the wind speed to perform random sampling, and PDFs and cumulative distribution functions (CDFs) of the SSO frequency and damping are obtained. The specific SSO probability assessment method steps are as follows:

*Step*1: Calculate the SSO frequency f_{sub} and the damping D at the given wind speed by eigenvalue analysis method based on the small signal model, and obtain the observation points (v_i, f_{subi}) $(i = 0, 1, 2, \ldots, m)$ and (v_i, D_i) $(i = 0, 1, 2, \ldots, m)$, respectively.

Step 2: Select the orthogonal basis function subspace, calculate the undetermined coefficients, and fit the LSM polynomial function forms of $f_{sub} = \varphi_f(v)$ and $D = \varphi_d(v)$ [30].

The orthogonal basis function subspace in this paper is $\Omega = span(1, x, \ldots, x^n)$, and the undetermined coefficients

of the fitting functions $f_{\text{sub}} = \varphi_{\text{f}}(v)$ and $D = \varphi_{\text{d}}(v)$ are respectively

$$\mathbf{a}_{\text{f}} = \left(\mathbf{B}^{\text{T}}\mathbf{B}\right)^{-1}\mathbf{B}^{\text{T}}\mathbf{f}$$

and

$$\mathbf{a}_{\text{d}} = \left(\mathbf{B}^{\text{T}}\mathbf{B}\right)^{-1}\mathbf{B}^{\text{T}}\mathbf{D}.$$

where $\mathbf{f} = (f_{\text{sub0}}, f_{\text{sub1}}, \ldots, f_{\text{sub}m})^{\text{T}}, \mathbf{D} = (D_0, D_1, \ldots, D_m)^{\text{T}}$, and

$$\mathbf{B}_{(m+1)\times(n+1)} = \begin{bmatrix} 1 & v_0 & \cdots & v_0^n \\ 1 & v_1 & \cdots & v_1^n \\ \vdots & \vdots & \ddots & \vdots \\ 1 & v_m & \cdots & v_m^n \end{bmatrix}.$$

$\mathbf{a}_{\text{f}} = (a_{\text{f0}}, a_{\text{f1}}, \ldots, a_{\text{fm}})^{\text{T}}, \mathbf{a}_{\text{d}} = (a_{\text{d0}}, a_{\text{d1}}, \ldots, a_{\text{dm}})^{\text{T}}$, n is the order of the fitting polynomial.

Then the fitting functions of the SSO frequency and damping are shown as (9) and (10), respectively.

$$\varphi_{\text{f}}(v) = \begin{cases} \sum_{j=0}^{n} a_{\text{f}j} v^j, & v \in [v_{\text{cut-in}}, v_{\text{rated}}] \\ \sum_{j=0}^{n} a_{\text{f}j} v_{\text{rated}}^j, & v \in (v_{\text{rated}}, v_{\text{cut-out}}] \end{cases} \tag{9}$$

$$\varphi_{\text{d}}(v) = \begin{cases} \sum_{j=0}^{n} a_{\text{d}j} v^j, & v \in [v_{\text{cut-in}}, v_{\text{rated}}] \\ \sum_{j=0}^{n} a_{\text{d}j} v_{\text{rated}}^j, & v \in (v_{\text{rated}}, v_{\text{cut-out}}] \end{cases} \tag{10}$$

Step 3: Introduce the probability distribution model of wind speed, generate the wind speed samples, and group the wind speed samples as a sequence $(v_1, v_2, \ldots, v_{\text{h}})$.

The two-parameter Weibull distribution [8] is used to describe the probability distribution of wind speed in this paper, which is the most widely used in many probabilistic models describing wind speed distribution. The wind speed obeys the two-parameter Weibull distribution, and the PDF is as follows:

$$f(v) = \left(\frac{k}{c}\right)\left(\frac{v}{c}\right)^{k-1}\exp\left[-\left(\frac{v}{c}\right)^k\right], \quad v \geq 0 \tag{11}$$

where, c and k are the scale parameter and the shape parameter of the Weibull distribution, respectively.

Based on the regional average wind speed μ and standard deviation δ, c and k can be solved by the following formulas.

$$k = \left(\frac{\delta}{\mu}\right)^{-1.068} \tag{12}$$

$$c = \frac{\mu}{\Gamma\left(1 + k^{-1}\right)} \tag{13}$$

where, $\Gamma(\cdot)$ is a Gamma function, whose expression is

$$\Gamma(x) = \int_0^{\infty} t^{x-1}\exp(-t)\,\mathrm{d}t \tag{14}$$

where, $x = 1 + k^{-1}$.

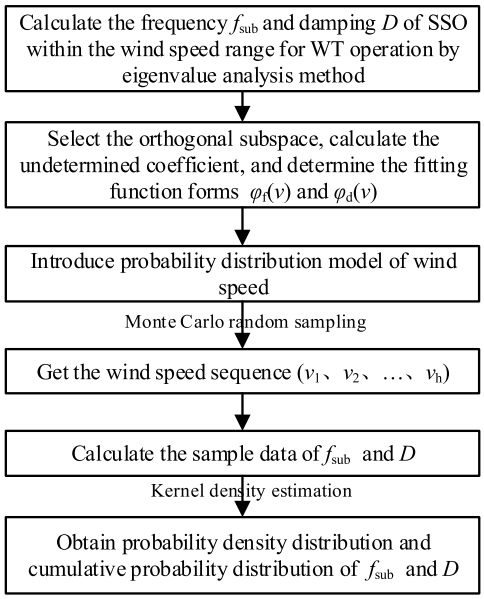

FIGURE 3. SSO frequency and damping probability assessment flow chart.

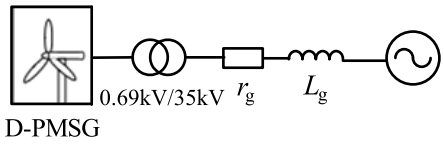

FIGURE 4. A single D-PMSG connected to grid.

With (11), a wind speed sample is obtained by Monte Carlo simulation [16], which is widely utilized to simulate random variables, shown as (15).

$$v = \left[c\left[-\ln(1-\xi)\right]^{1/k}\right] \tag{15}$$

where, ξ is a random number that follows uniform distribution on the interval [0, 1].

Step 4: Input the wind speed samples, calculate the SSO frequency and the damping sample values according to (9) and (10), respectively, and obtain the PDF and CDF of f_{sub} and D based on kernel density estimation [18].

The complete flow chart is given in Fig. 3.

IV. ANALYSIS AND SIMULATION FOR IMPACTS OF WIND SPEED CHANGE ON SSO

A. ANALYSIS BASED ON EIGENVALUE METHOD

The system of a single D-PMSG connected to a grid is shown in Fig. 4. GW/1500, the typical model of D-PMSG used in the wind farms in Hami, China is taken as the research object. The main parameters of the system are given in Table 1.

The small signal model is established under the given parameters in Table 1. Based on the eigenvalue analysis method, the oscillation frequency f_{os1} and damping D_1 of the system in dq frame under different wind speed conditions are obtained as shown in Table 2.

TABLE 1. Parameters of D-PMSG AC grid-connected system.

Parameters	Value
Rated power	1.5MW
Rated voltage	0.69kV
DC-side capacitor	C_{dc}=35mF
Filter inductor	L_1=0.4mH
Grid connection reactance	L_g=0.5146H
Grid connection resistance	$r_g = 0$
System's capacity base value	1.5MVA.
DC link rated voltage	1.1kV
Rated wind speed	11 m/s
Cut-in wind speed	3 m/s
Cut-out wind speed	22 m/s

TABLE 2. Oscillation characteristics of the system in DQ frame under different wind speeds.

Wind speed (m/s)	P_s (pu)	Frequency f_{os1}(Hz)	Damping D_1 (s^{-1})
3	0.020 2	28.993 6	-1.821 8
3.5	0.032 2	28.994 7	-1.544 8
4	0.048 0	28.995 5	-1.176 3
4.5	0.068 4	28.995 2	-0.703 5
5	0.093 9	28.992 9	-0.113 6
5.5	0.125 0	28.987 1	0.606 9
6	0.162 2	28.975 8	1.469 7
6.5	0.206 3	28.956 3	2.487 4
7	0.257 7	28.925 1	3.671 9
7.5	0.316 9	28.877 8	5.034 6
8	0.384 6	28.808 7	6.586 0
8.5	0.461 4	28.710 6	8.335 5
9	0.547 7	28.574 6	10.290 7
9.5	0.644 1	28.389 4	12.456 6
10	0.751 3	28.140 5	14.834 2
10.5	0.869 7	27.809 6	17.417 9
11	1.000 0	27.372 2	20.191 3

In Table 2, it can be seen that as the wind speed increases, the output power of the D-PMSG increases, the damping D_1 increases, and the oscillation frequency f_{os1} decreases slightly. Since the SSO frequency $f_{sub1} = 50 - f_{os1}$, as the wind speed increases, the SSO frequency increases slightly as the same presentation in [2]. Although there is a slight increase of the oscillation frequency f_{os1} from 3 m/s to 4 m/s shown in Table 2, it is negligible relative to the overall change trend.

B. PSCAD SIMULATION VERIFICATION

The aforementioned eigenvalue analysis results based on the proposed small signal model are verified with the time-domain simulations in the PSCAD/EMTDC environment.

The simulation of the system shown in Fig. 4 is performed. The initial wind speed is set to 8 m/s, and it is changed to 7 m/s and 5 m/s at 40s, respectively. The dynamic curves of phase A current and active power of the Point of Common Coupling (PCC) under the two wind speed change conditions are shown in Figs. 5-6, respectively.

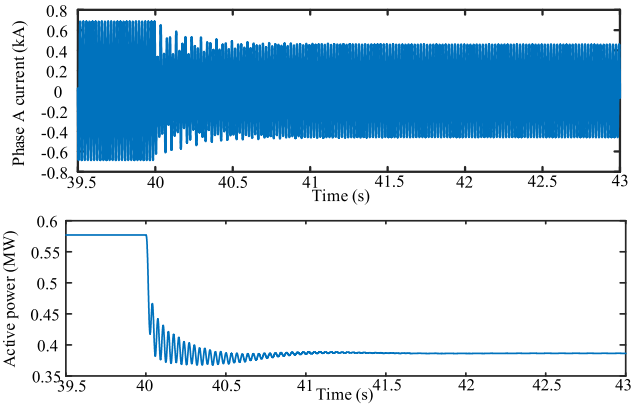

FIGURE 5. Current and active power at PCC when wind speed changes from 8 m/s to 7 m/s at 40s.

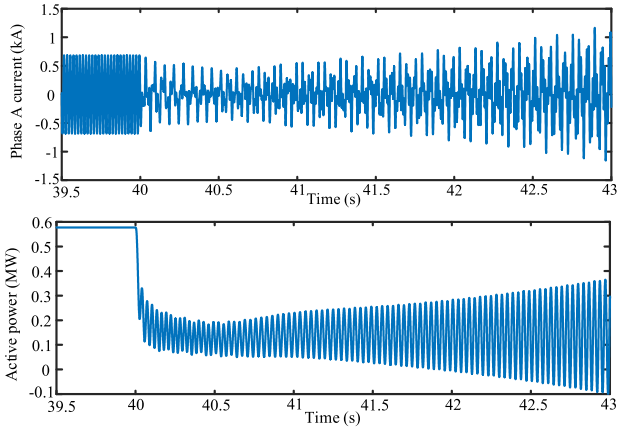

FIGURE 6. Current and active power at PCC when wind speed changes from 8 m/s to 5 m/s at 40s.

According to Fig. 5, when the wind speed changes from 8 m/s to 7 m/s, both the current and the active power at PCC decrease, and reach a stable state after a slight oscillation. Fig. 6 shows that when the wind speed changes from 8 m/s to 5 m/s, the current at PCC decreases, causing the severe distortion and the divergence; the active power firstly decreases, and then rapidly oscillates and diverges.

In order to observe and compare the operating states of system under different wind speeds, the wind speed changes from 8 m/s to 7 m/s, 6 m/s, 5 m/s, 4 m/s and 3 m/s, respectively. The comparison of the active power curves at PCC under the different wind speed changes is shown in Fig. 7.

As can be seen from Fig. 7, when the wind speed changes from 8 m/s to 7 m/s and 6 m/s, the oscillations converge, and the convergence rate of 7 m/s is faster than that of 6 m/s. When the wind speed changes from 8 m/s to 5 m/s, 4 m/s, and 3 m/s, the oscillations diverge, and the divergence rate of 5 m/s is the slowest, and the divergence rate of 3m/s is the fastest. The active power oscillation curves in Fig. 7 are analyzed by Prony algorithm [31], and the oscillation frequency f_{os2} and damping D_2 are obtained as shown in Table 3.

In Table 3, it can be seen that as the wind speed increases, the oscillation frequency f_{os2} decreases slightly, the corresponding to SSO frequency $f_{sub2} = 50 - f_{os2}$ increases

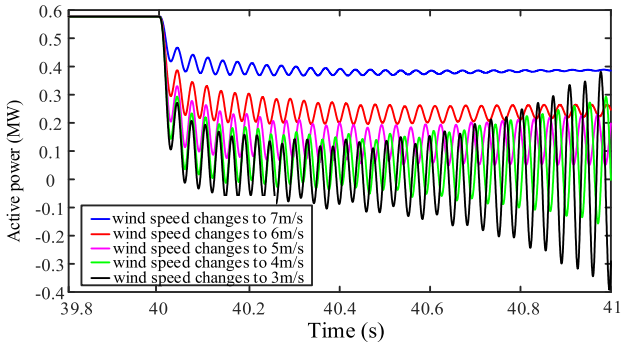

(a) Before filtering out the DC component

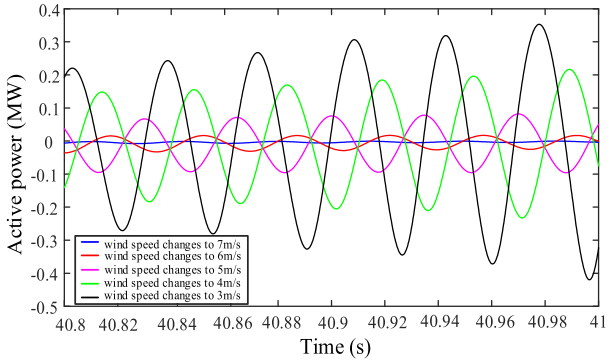

(b) Partial enlargement after filtering out the DC component

FIGURE 7. Active power curves when the wind speed changes from 8 m/s to different the lower wind speeds.

TABLE 3. Results of PSCAD simulation under different wind speeds.

Wind Speed (m/s)	Frequency fos_2 (Hz)	Damping D_2 (s^{-1})
3	29.053 2	-1.815 7
4	29.046 1	-1.189 4
5	28.992 6	-0.111 9
6	28.982 5	1.436 4
7	28.953 4	3.781 8

slightly, and the damping is enhanced, which are consistent with the conclusions based on eigenvalue analysis. Comparing of the data corresponding different wind speeds in Table 2 and Table 3, it can be seen that the oscillation frequencies and dampings obtained by time-domain simulation are close to those of the eigenvalue analysis, and the errors are all less than 2%, which validates the accuracy of the small signal model.

V. CASE STUDIES FOR SSO PROBABILITY ASSESSMENT

With the data of SSO frequencies and dampings under 3.5 m/s, 5 m/s, 6 m/s, 7 m/s, 9.5 m/s and 10.5 m/s in Table 1 and Table 4, the functions of $f_{sub} = \varphi_f(v)$ and $D = \varphi_d(v)$ are obtained with LSM polynomial curve fitting, selecting the orthogonal basis function subspace $\Omega = span(1, v, v^2, v^3, v^4)$, and the redundancy 1. Then set the average wind speed $\mu = 4$ m/s, $\mu = 6$ m/s, $\mu = 8$ m/s,

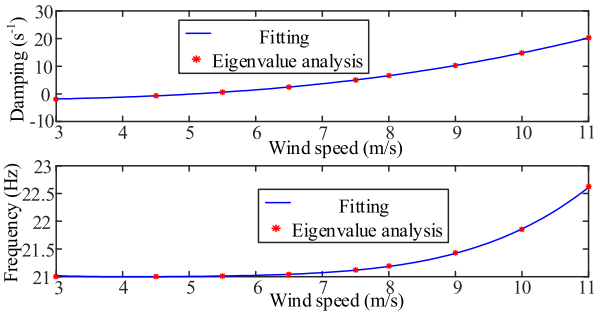

FIGURE 8. Comparison of eigenvalue analysis results with fitting results.

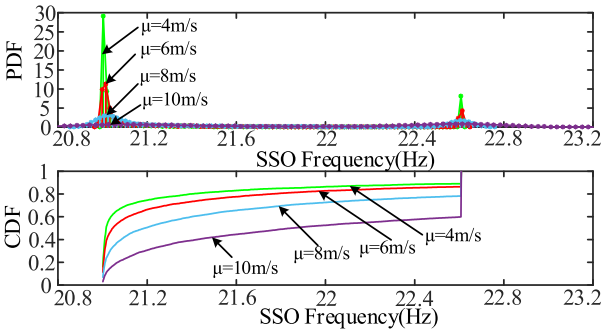

FIGURE 9. PDFs and CDFs of SSO frequency under different average wind speeds.

$\mu = 10$ m/s, respectively, and the standard deviation $\delta = 3.7$ [8] of the location of D-PMSG-based WPGS, and obtain the probability density Weibull distribution function of the wind speed according to (11)-(14). Then use the Monte Carlo method to randomly extract 8000 samples of the wind speed, and the PDFs and CDFs of the SSO frequency and damping caused by the change of wind speed under one D-PMSG and multiple D-PMSGs scenarios are obtained based on the proposed assessment method shown in Fig. 3.

A. INFLUENCE OF WIND SPEED ON SSO PROBABILITY DISTRIBUTION OF ONE D-PMSG

For the case of a single D-PMSG connected to grid shown in Fig. 4, the relationships $f_{sub} = \varphi_f(v)$ and $D = \varphi_d(v)$ are obtained based on LSM polynomial curve fitting, compared with the results obtained by eigenvalue analysis method, as shown in Fig. 8.

The sum of squared errors (SSE) between the damping and wind speed fitting curve results and the eigenvalue analysis results is 0.0128; the SSE between the SSO frequency and wind speed fitting curve results and the eigenvalue analysis results is 0.0077. Observing the fitting of Fig. 8 and the SSEs of SSO damping and frequency, the functions of $f_{sub} = \varphi_f(v)$ and $D = \varphi_d(v)$ are obtained accurately with LSM polynomial curve fitting.

Since the average values of wind speeds are different in different months, the PDFs and CDFs of f_{sub} and D under different average wind speeds are compared and analyzed as shown in Fig. 9 and Fig. 10.

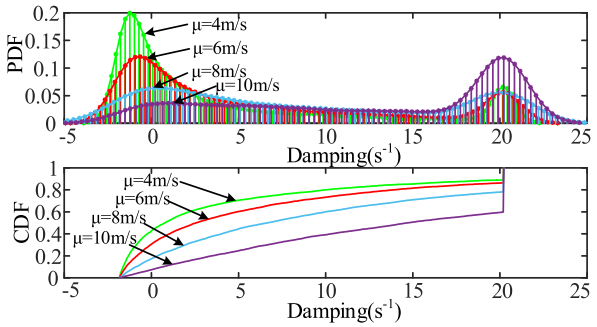

FIGURE 10. PDFs and CDFs of SSO damping under different average wind speeds.

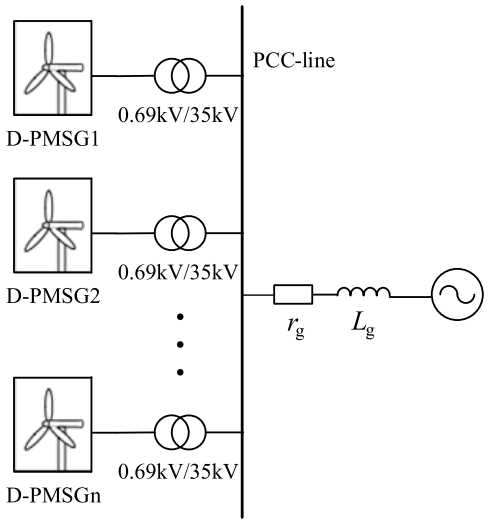

FIGURE 11. Multiple D-PMSGs connected to grid.

It can be seen from Fig. 9 that the decrease of the average wind speed makes the gravity center of the probability density distribution of the SSO frequency move from a region with high SSO frequency to a region with low SSO frequency, that is, the possibility of generating a slightly lower SSO frequency is greater. As can be seen from Fig. 10, the decrease of the average wind speed makes the gravity center of the probability density distribution of the SSO damping gradually move from the larger damping area to the smaller damping area, that is, the probability of negative damping increases and the risk of unstable SSO is higher. It can be seen from Figs. 9-10 that when the system is running at rated power, the SSO frequency and damping are 22.6Hz and 20.2s^{-1}, respectively, and the probability of the system operating at rated power reduces as the average wind speed decreases.

B. INFLUENCE OF WIND SPEED ON SSO PROBABILITY DISTRIBUTION UNDER DIFFERENT NUMBER OF D-PMSGS

The system of multiple D-PMSGs connected to the grid is set up as shown in Fig. 11. The grid connection reactance L_g is 1.47mH, and the remaining D-PMSG parameters and circuit parameters are the same as those in Fig. 4. Grid-connected scenarios of 300, 500 and 750 sets of D-PMSGs are selected

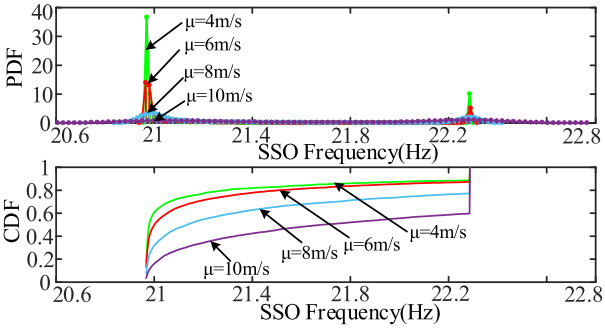

FIGURE 12. PDFs and CDFs of SSO frequency for 300 D-PMSGs at different average wind speeds.

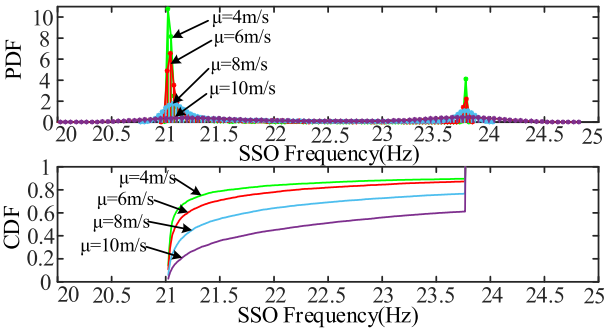

FIGURE 13. PDFs and CDFs of SSO frequency for 500 D-PMSGs at different average wind speeds.

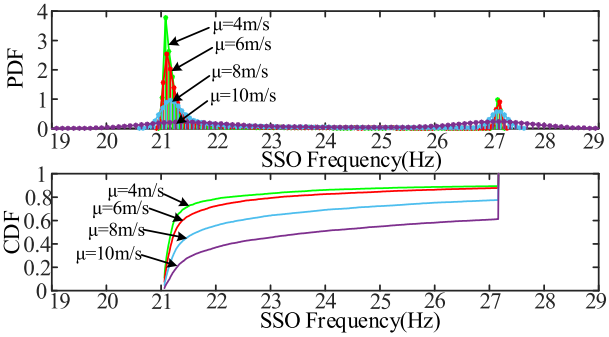

FIGURE 14. PDFs and CDFs of SSO frequency for 750 D-PMSGs at different average wind speeds.

to study the influence of wind speed variation on the SSO characteristics and the probability assessment is conducted.

First, the functional relationships $f_{sub} = \varphi_f(v)$ and $D = \varphi_d(v)$ are accurately obtained under the different number of D-PMSGs connected to grid, as shown in Figs. 21, 22, and 23. Then calculate the PDFs and CDFs of the SSO frequency and damping with different average wind speeds under the different number of D-PMSGs scenarios.

The PDFs and CDFs of SSO frequency are as shown in Figs.12-14. From Figs. 12-14 and Table 4, when 300, 500, and 750 sets of D-PMSGs are connected to the grid, the SSO frequency ranges are 20.93Hz to 22.30Hz, 21.03Hz to 23.83Hz and 21.10Hz to 27.20Hz, respectively, and the bandwidths are 1.37Hz, 2.8 Hz and 6.1 Hz, respectively, caused by the same wind speed variations. Therefore, the variation range

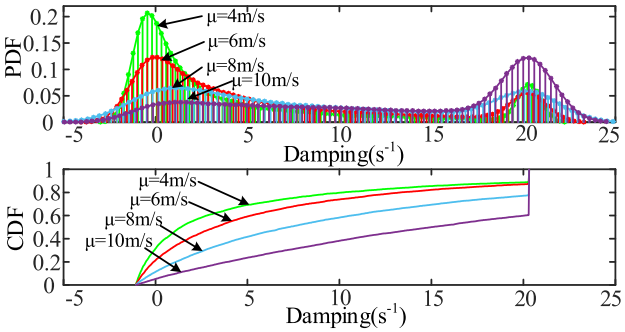

FIGURE 15. PDFs and CDFs of SSO damping for 300 D-PMSGs at different average wind speeds.

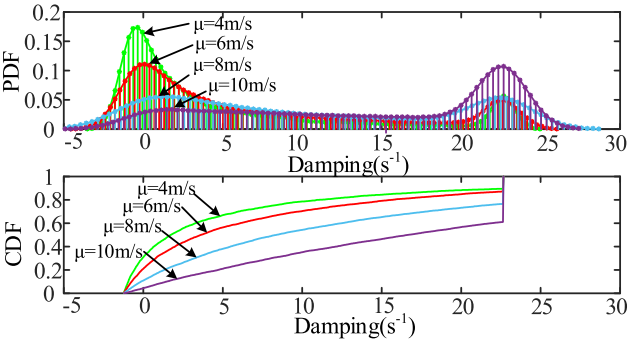

FIGURE 16. PDFs and CDFs of SSO damping for 500 D-PMSGs at different average wind speeds.

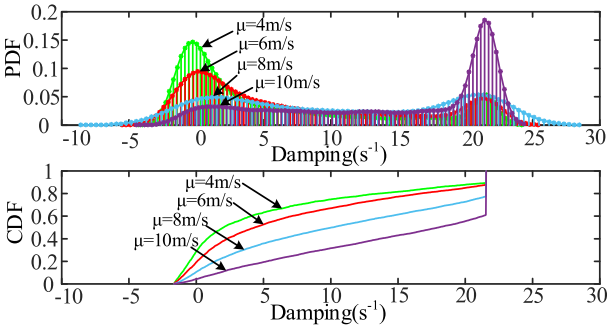

FIGURE 17. PDFs and CDFs of SSO damping for 750 D-PMSGs at different average wind speeds.

of the SSO frequency becomes larger with the increase of the number of D-PMSGs connected to grid. Under the same average wind speed, the increase of the number of grid-connected D-PMSGs makes the gravity center of the probability density distribution of SSO frequency gradually move from a region with low SSO frequency to a region with high SSO frequency, that is, the possibility of generating a higher SSO frequency is greater.

The PDFs and CDFs of SSO damping are shown in Figs.15-17. The probability of unstable SSO under different average wind speeds with the different number of D-PMSGs connected to grid can be known from Figs. 15-17. As for an example, it can be seen from Fig. 17 that in the scenario where 750 sets of D-PMSGs are connected to the grid, when the average wind speed is 4 m/s, 6 m/s, 8 m/s,

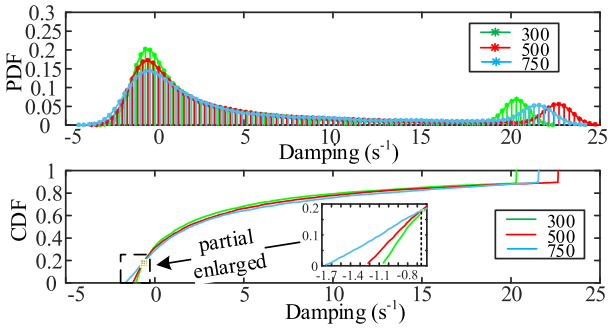

FIGURE 18. PDFs and CDFs of SSO damping under the different number of D-PMSGs in the case of average wind speed μ = 4m/s.

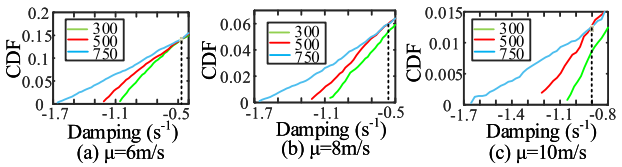

FIGURE 19. Partial enlargement of the damping CDFs.

and 10 m/s, the estimated probability of negative damping is 29.26%, 20.44%, 10.19%, and 4.13%, respectively. Therefore, under a certain number of D-PMSGs connected to a grid, the smaller the average wind speed is, the bigger the risk of the system to generate unstable SSO is.

In order to better compare the influences of different number of D-PMSGs on the damping probability distribution, the PDFs and CDFs of SSO damping in the same average wind speed with different number of D-PMSGs are placed in one graph respectively. For instance, the graphs of μ = 4 m/s are shown in Fig. 18 with an enlarged view of the dotted rectangle. When the average wind speed μ is 6 m/s, 8 m/s, and 10 m/s, the enlarged views of the cumulative probability distributions corresponding to the portion of the dotted rectangle in Figs. 15-17 are shown in Fig. 19.

Comparing Fig. 14 with Fig. 18, the average wind speed has a greater influence on the probability distribution of SSO damping than that of the number of D-PMSGs. Known from Figs. 18-19, under the system parameters, when the dampings are less than -0.66s^{-1}, -0.47s^{-1}, -0.56s^{-1} and -0.90s^{-1}, corresponding to the average wind speeds μ is 4 m/s, 6 m/s, 8 m/s, and 10 m/s, respectively, the probability of unstable SSO increases with the increase of the number of D-PMSGs connected to grid.

When μ is 4 m/s, the PDFs and CDFs of SSO frequency with different number of D-PMSGs are placed in one graph respectively shown in Fig. 20. Comparing Fig. 18 with Fig. 20, it can be seen that the change of D-PMSGs number has a greater influence on the SSO frequency than damping.

In July 2015, the average wind speed in Hami was about 4 m/s, and the real-time SSO frequency of fluctuation range and bandwidth are showed in Fig. 1 [3]. Considering the SSO frequency value, the frequency variation range and the prob-

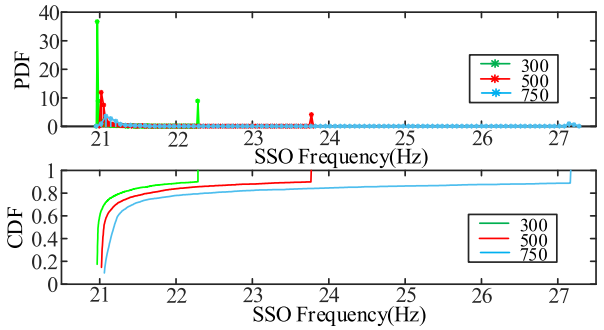

FIGURE 20. PDFs and CDFs of SSO frequency under the different number of D-PMSGs in the case of average wind speed $\mu = 4$ m/s.

ability of unstable SSO when the average wind speed is 4 m/s under the 750 D-PMSGs connected to grid scenario, it can be seen that the parameters of the scenario can better match the actual scene in Hami area. Therefore, the effectiveness of the proposed method is verified.

VI. CONCLUSION

The main contributions of this paper are:

1) A small signal model that accounts for wind speed is established using the functional relationship between wind speed and output power of WT. The LSM polynomial method is used to accurately obtain the functions of $\varphi_f(v)$ and $\varphi_d(v)$ in the wind speed range under the different number of D-PMSGs, and the influence of the change of wind speed on the SSO frequency and damping are quantitatively analyzed under the different number of D-PMSGs scenarios.

2) Within the wind speed range for WT operation, the SSO probability assessment method is proposed with the introduce of the probability distribution of wind speed, and the PDFs and CDFs of SSO frequency and damping are obtained under different number of D-PMSGs and different average wind speed scenarios. This work achieves an efficient SSO time-varying characteristics probability assessment, and the PDFs of SSO frequency and the risk of unstable SSO provide guidance for suppression solutions.

3) The variation range of SSO frequency in the actual accident scenario in Hami, China is reproduced.

The main conclusions are obtained as follows:

1) In the wind speed range for WT operation, when the number of D-PMSGs connected to grid is constant, as the average wind speed decreases, the gravity center of the probability density distribution of the SSO frequency of D-PMSG-based WPGS gradually moves to the small value region, that is, the possibility of generating SSO with lower frequency is greater; at the same time, the probability density distribution of the SSO damping gradually moves toward the region where the damping is weak, that is, the probability of unstable SSO increases.

2) Under the same average wind speed, when the number of D-PMSGs connected to grid increases, the gravity center of probability density distribution of the SSO frequency gradually shifts to a large value region, that is, the possibility of generating SSO with higher frequency is greater; the increase of the number of D-PMSGs connected to grid makes the SSO frequency variation range increase significantly; to a certain small extent of the negative damping, the probability of unstable SSO becomes larger with the increase of the number of D-PMSGs connected to grid.

3) Comparison of the influence of the average wind speed and the number of D-PMSGs on SSO characteristics of D-PMSG-based WPGS: the change of D-PMSGs number has a greater influence on the probability distribution of SSO frequency than damping, the average wind speed has a greater influence on the probability distribution of SSO damping than that of the number of D-PMSGs.

APPENDIX A

TABLE 4. Oscillation characteristics of the system in DQ frame under different wind speeds and different D-PMSGs number.

Wind speed (m/s)	P_s (pu)	300		500		750	
		Frequency f_{sub1}(Hz)	Dampling D_1 (s^{-1})	Frequency f_{sub2}(Hz)	Dampling D_1 (s^{-1})	Frequency f_{sub3}(Hz)	Dampling D_1 (s^{-1})
3	0.020 3	20.970 8	-1.057 7	21.032 1	-1.183 1	21.102 5	-1.324 2
3.5	0.032 2	20.967 0	-0.791 1	21.031 0	-0.873 2	21.101 1	-0.964 7
4	0.048 1	20.969 4	-0.436 5	21.030 7	-0.461 2	21.101 3	-0.486 9
4.5	0.068 5	20.969 7	0.018 7	21.032 2	0.067 6	21.105 0	0.125 8
5	0.093 9	20.971 7	0.586 8	21.037 3	0.727 1	21.115 2	0.889 5
5.5	0.125 0	20.976 6	1.280 2	21.048 2	1.531 6	21.135 9	1.819 5
6	0.162 3	20.986 2	2.111 1	21.068 1	2.494 4	21.173 0	2.930 6
6.5	0.206 3	21.002 5	3.091 5	21.101 4	3.628 8	21.234 3	4.236 0
7	0.257 7	21.028 5	4.233 1	21.153 7	4.947 0	21.330 0	5.746 8
7.5	0.317 0	21.068 0	5.547 2	21.232 3	6.460 1	21.474 1	7.470 5
8	0.384 7	21.125 5	7.044 5	21.346 6	8.177 2	21.685 0	9.408 9
8.5	0.461 4	21.206 8	8.734 9	21.508 7	10.104 8	21.988 0	11.554 0
9	0.547 7	21.319 4	10.627 1	21.734 3	12.244 7	22.419 0	13.879 5
9.5	0.644 2	21.472 1	12.727 9	22.044 3	14.591 4	23.030 9	16.322 6
10	0.751 3	21.676 4	15.041 6	22.466 7	17.126 4	23.909 4	18.736 8
10.5	0.869 7	21.946 3	17.568 2	23.040 9	19.807 2	25.209 9	20.741 4
11	1.000 0	22.300 3	20.301 5	23.825 4	22.542 2	27.274 5	21.0295

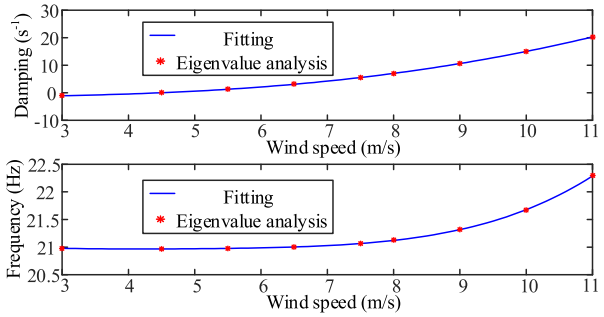

FIGURE 21. Comparison of eigenvalue analysis results with fitting results of 300 D-PMSGs.

APPENDIX B

Known from the Figs. 21, 22, and 23, the curves obtained by fitting the LSM polynomial curve in the grid-connected scenarios of 300, 500, and 750 D-PMSGs accurately fit the relationship between wind speed and SSO frequency or damping.

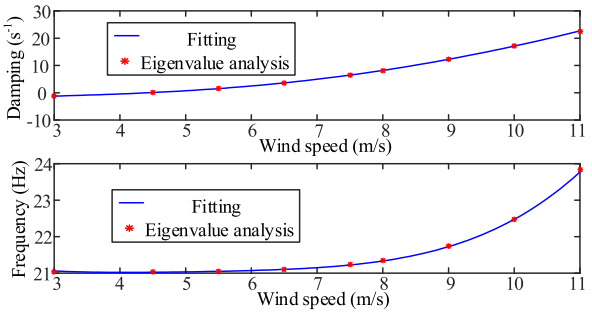

FIGURE 22. Comparison of eigenvalue analysis results with fitting results of 500 D-PMSGs.

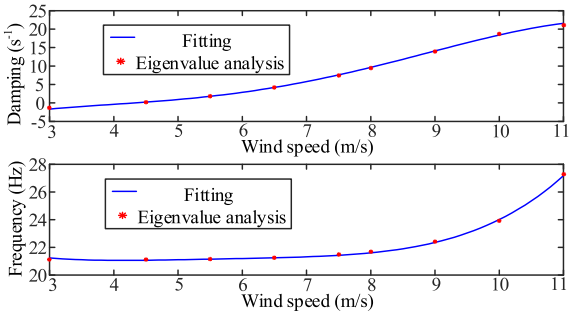

FIGURE 23. Comparison of eigenvalue analysis results with fitting results of 750 D-PMSGs.

REFERENCES

[1] G. M. Shafiullah, A. M. T. Oo, A. B. M. S. Ali, and P. Wolfs, "Potential challenges of integrating large-scale wind energy into the power grid—A review," *Renew. Sustain. Energy Rev.*, vol. 20, pp. 306–321, Apr. 2013.

[2] X. Xie, H. Liu, J. He, C. Zhang, and Y. Qiao, "Mechanism and characteristics of subsynchronous oscillation caused by the interaction between full-converter wind turbines and AC systems," *Proc. CSEE*, vol. 36, no. 9, pp. 2366–2372, May 2016.

[3] M. Li, Z. Yu, T. Xu, J. He, C. Wang, X. Xie, and C. Liu, "Study of complex oscillation caused by renewable energy integration and its solution," *Power Syst. Technol.*, vol. 41, no. 4, pp. 1035–1042, Apr. 2017.

[4] H. Liu, X. Xie, J. He, T. Xu, Z. Yu, C. Wang, and C. Zhang, "Subsynchronous interaction between direct-drive PMSG based wind farms and weak AC networks," *IEEE Trans. Power Syst.*, vol. 32, no. 6, pp. 4708–4720, Nov. 2017.

[5] X. Wang, W. Du, and H. Wang, "Mechanism analysis of instability caused by dynamic interactions between converter control systems in PMSG based wind farms," *Power Syst. Technol.*, vol. 42, no. 8, pp. 2423–2430, Aug. 2018.

[6] K. Y. Liao, S. Tao, and L. T. Yao, "Study on frequency-domain modeling and time-varying characteristics of DFIG input impedance with excitation under static reference frame," *Proc. CSEE*, vol. 38, no. 16, pp. 4886–4897 and 4994, Jan. 2018.

[7] X. Guo, R. Gong, and H. Bao, "Modeling of wind speed uncertainty based on evidence theory," *Electr. Power Autom. Equip.*, vol. 39, no. 1, pp. 78–83, Jan. 2019.

[8] W. Chen, D. Wang, R. Su, P. Dong, L. Tan, and Y. Yu, "Risk-based security assessment method of IGE caused by doubly-fed wind farms," *Power Syst. Technol.*, vol. 41, no. 3, pp. 854–862, Mar. 2017.

[9] Y. Cheng, M. Sahni, D. Muthumuni, and B. Badrzadeh, "Reactance scan crossover-based approach for investigating SSCI concerns for DFIG-based wind turbines," *IEEE Trans. Power Del.*, vol. 28, no. 2, pp. 742–751, Apr. 2013.

[10] Y. Huang, X. Wang, and K. Chen, "SSI mechanism simulation validation and practical mitigation strategy of DFIG-based wind farms," *Power Syst. Technol.*, vol. 40, no. 8, pp. 2364–2369, Aug. 2016.

[11] X. Dong, X. Xie, J. Li, and Y. Han, "Comparative study of the impact on subsynchronous resonance characteristics from the different location of wind generators in a large wind farm," *Proc. CSEE*, vol. 35, no. 20, pp. 5173–5180, Jun. 2015.

[12] L. Fan and Z. Miao, "Nyquist-stability-criterion-based SSR explanation for type-3 wind generators," *IEEE Trans. Energy Convers.*, vol. 27, no. 3, pp. 807–809, Sep. 2012.

[13] R. Song, J. Guo, B. Li, P. Zhou, N. Du, and D. Yang, "Mechanism and characteristics of subsynchronous oscillation in direct-drive wind power generation system based on input-admittance analysis," *Proc. CSEE*, vol. 37, no. 16, pp. 4662–4670, Aug. 2017.

[14] S. Chen, Y. Cao, and Q. Jiang, *Theory and Method of Sub-Synchronous Oscillation of Electrical Power System*. Beijing, China: Science Press, 2009, pp. 148–163.

[15] X. Peng, L. Xiong, J. Wen, S. Cheng, D. Deng, S. Feng, and B. Wang, "A summary of the state of the art for short-term and ultra-short-term wind power prediction of regions," *Proc. CSEE*, vol. 36, no. 23, pp. 6315–6326, Dec. 2016.

[16] W. P. Wu, Z. C. Hu, and Y. H. Song, "Optimal sizing of energy storage system for wind farms combining stochastic programming and sequential Monte Carlo simulation," *Power Syst. Technol.*, vol. 42, no. 4, pp. 1055–1062, Apr. 2018.

[17] Z. Liu, Z. Wei, G. Sun, H. Zang, and Y. Li, "Probabilistic power flow calculation of power system with wind farms considering fuzzy parameters," *Power Syst. Technol.*, vol. 41, no. 7, pp. 2308–2315, Jul. 2017.

[18] L. Ye, Y. Zhang, Y. Ju, X. Song, Y. Lang, and Q. Li, "Gaussian mixture model for probabilistic power flow calculation of system integrated wind farm," *Proc. CSEE*, vol. 37, no. 15, pp. 4379–4387, Aug. 2017.

[19] Y. Ma, J. Liu, and J. Yan, "Small disturbance stability analysis of power system containing wind power based on stochastic response surface method," *Trans. China Electrotech. Soc.*, vol. 32, no. 6, pp. 49–57, Mar. 2017.

[20] R. Preece, K. Huang, and J. V. Milanović, "Probabilistic small-disturbance stability assessment of uncertain power systems using efficient estimation methods," *IEEE Trans Power Syst.*, vol. 29, no. 5, pp. 2509–2517, Sep. 2014.

[21] X. Bian, L. Shi, Q. Zhou, and Y. Fu, "Sub-synchronous interaction and its suppression measurement caused by grid-integration of DFIG-based wind farms using probabilistic method," *High Voltage Eng.*, vol. 42, no. 9, pp. 2740–2747, Sep. 2016.

[22] X. Bian, L. Shi, X. Zong, D. Li, and Y. Fu, "Analysis and mitigation of wind turbine converters in sub-synchronous interaction under multi-operating conditions," *Trans. China Electrotech. Soc.*, vol. 32, no. 11, pp. 38–47, Jun. 2017.

[23] Z. An, C. Shen, Z. Zheng, F. Liu, X. Chang, and W. Wei, "Scenario-based analysis and probability assessment of sub-synchronous oscillation caused by wind farms with direct-driven wind generators," *J. Mod. Power Syst. Clean Energy*, vol. 7, no. 2, pp. 243–253, Mar. 2019.

[24] S. Huang, J. Gao, and D. Luo, *Direct Drive Permanent Magnet Wind Turbine Design and Grid Control*. Beijing, China: Electronics Industry, 2014, pp. 22–23.
[25] C. Zhang, W. Wang, G. He, G. Li, H. Wang, and Y. Tian, "Analysis of sub-synchronous oscillation of full-converter wind farm based on sequence impedance and an optimized design method for PLL parameters," *Proc. CSEE*, vol. 37, no. 23, pp. 6757–6767, Dec. 2017.
[26] J. Sun, "Impedance-based stability criterion for grid-connected inverters," *IEEE Trans. Power Electron.*, vol. 26, no. 11, pp. 3075–3078, Nov. 2011.
[27] X. Wang, L. Harnefors, and F. Blaabjerg, "Unified impedance model of grid-connected voltage-source converters," *IEEE Trans. Power Electron.*, vol. 33, no. 2, pp. 1775–1787, Feb. 2018.
[28] W. Liu and J. Jiang, "Modeling and analysis for direct-drive permanent magnet synchronous wind turbine generator in subsynchronous oscillation," *Motor Control Appl.*, vol. 44, no. 1, pp. 97–103, Jan. 2017.
[29] K. M. Alawasa, Y. A.-R. I. Mohamed, and W. Xu, "Active mitigation of subsynchronous interactions between PWM voltage-source converters and power networks," *IEEE Trans. Power Electron.*, vol. 29, no. 1, pp. 121–134, Jan. 2014.
[30] M. Kesäniemi and K. Virtanen, "Direct least square fitting of hyperellipsoids," *IEEE Trans. Pattern Anal. Mach. Intell.*, vol. 40, no. 1, pp. 63–76, Jan. 2018.
[31] H. Xue and P. Zhang, "Subspace-least mean square method for accurate harmonic and interharmonic measurement in power systems," *IEEE Trans. Power Del.*, vol. 27, no. 3, pp. 1260–1267, Jul. 2012.

SHUN TAO was born in China, in November 1972. She received the M.S. and Ph.D. degrees from North China Electric Power University (NCEPU), in 2005 and 2008, respectively.

She had a Postdoc Procedure at the Electrical Engineering Laboratory de Grenoble (G2Elab), Institute National Polytechnique de Grenoble (INPG), Grenoble, France, in 2010. She has been with the NCEPU, since 2008. Her research interests include active distribution network and its power-quality.

LEI ZHAO was born in Hengshui, Hebei, China, in 1995. She received the B.S. degree in electrical engineering and automation from Hebei University, Baoding, China, in 2017. She is currently pursuing the M.S. degree with the Institute of State Key Laboratory for Alternate Electrical Power System with Renewable Energy Sources, Beijing, China.

Her research interests include power quality and sub-synchronous oscillation in the power system with PMSG.

KUNYU LIAO was born in Xuchang, Henan, China, in 1989. He received the B.S. degree in electrical engineering and automation from the Huazhong University of Science and Technology, Wuhan, China, in 2013, and the Ph.D. degree in electrical engineering from the State Key Laboratory of Alternate Electrical Power System With Renewable Energy Sources, North China Electric Power University, Beijing, China, in 2019.

His research interests include the modeling analysis and suppression of power quality and sub-synchronous oscillation in the power system with renewable energy sources.

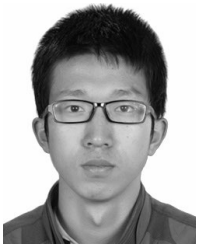

YUNBO LIU was born in Jilin, China. He received the Bachelor of Engineering degree from the College of Electrical and Electronic Engineering, North China Electric Power University, Beijing, China, in 2018, where he is currently pursuing the M.S. degree in electrical engineering. His current research interests include the control system and the power quality of wind power generation.